Annals of Biomedical Engineering
https://doi.org/10.1007/s10439-023-03217-x

BMES BIOMEDICAL ENGINEERING SOCIETY

ORIGINAL ARTICLE

Hip and Knee Joint Kinematics Predict Quadriceps Hyperreflexia in People with Post-stroke Stiff-Knee Gait

Jeonghwan Lee[1] · Tunc Akbas[2] · James Sulzer[3]

Received: 11 November 2022 / Accepted: 20 April 2023

Abstract

Wearable assistive technology for the lower extremities has shown great promise towards improving gait function in people with neuromuscular injuries. But common secondary impairments, such as hypersensitive stretch reflexes or hyperreflexia, have been often neglected. Incorporation of biomechanics into the control loop could improve individualization and avoid hyperreflexia. However, adding hyperreflexia prediction to the control loop would require expensive or complex measurement of muscle fiber characteristics. In this study, we explore a clinically accessible biomechanical predictor set that can accurately predict rectus femoris (RF) reaction after knee flexion assistance in pre-swing by a powered orthosis. We examined a total of 14 gait parameters based on gait kinematic, kinetic, and simulated muscle–tendon states from 8 post-stroke individuals with Stiff-Knee gait (SKG) wearing a knee exoskeleton robot. We independently performed both parametric and non-parametric variable selection approaches using machine learning regression techniques. Both models revealed the same four kinematic variables relevant to knee and hip joint motions were sufficient to effectively predict RF hyperreflexia. These results suggest that control of knee and hip kinematics may be a more practical method of incorporating quadriceps hyperreflexia into the exoskeleton control loop than the more complex acquisition of muscle fiber properties.

Keywords Stroke · Gait · Exoskeletons · Biomechanics · Wearable sensors · Spasticity · Reflex

Introduction

Gait disorders are common in stroke survivors. More than 80% of stroke survivors have varying degrees of gait abnormalities [14, 24], and about 25% have a residual impairment that requires full physical assistance, despite rehabilitation efforts [20]. Recent technological advances have introduced wearable robots as potential solutions to mitigate physical barriers for people with impaired mobility. There are various commercialized and research purpose lower-body exoskeletons showing promise in performance augmentation, mobility assistance, and gait therapy following neurological injuries [15, 46]. Assistive strategies using exoskeletons incorporate force, torque, electromyography (EMG), and gait kinematics into the control loop [25, 46]. For example, a human-in-the-loop approach with ankle exoskeletons in healthy individuals controlled kinematic and kinetic parameters correlated with metabolic cost, finding a substantial reduction in metabolic cost and increased self-selected speed [40]. Human-in-the-loop approaches in clinical populations remains on the frontier [39]. Further, exoskeletal development has largely ignored addressing critical neuromuscular impairments such as hyperreflexia, defined as a hypersensitive stretch reflex.

Hyperreflexia is a supposed mechanism of Stiff-Knee gait (SKG), a common abnormal gait pattern following stroke characterized by diminished knee flexion during the swing phase of the gait cycle [32]. We previously developed a lightweight, remotely actuated powered knee orthosis [43] to assist post-stroke individuals with SKG. This robotic knee exoskeleton was expected to improve swing phase knee flexion kinematics. Knee flexion velocity increased in

Associate Editor Thurmon E. Lockhart oversaw the review of this article.

✉ James Sulzer
jss280@case.edu

[1] Walker Department of Mechanical Engineering, University of Texas at Austin, Austin, TX, USA

[2] Intel Corporation, Hillsboro, OR, USA

[3] Department of Physical Medicine and Rehabilitation, MetroHealth Medical Center and Case Western Reserve University, Cleveland, OH, USA

Published online: 03 May 2023

early swing, but those gains were counteracted by a hyperreflexia response in the rectus femoris (RF) that brakes the knee, a reaction made more common by assistance [2]. In a different cohort of individuals with post-stroke SKG, reflex excitability of the RF was measured with peripheral nerve stimulation (H-reflex) during the pre-swing phase of walking [1]. We found a negative correlation between individuals with RF reflex excitability and pre-swing knee flexion angle [1]. Taken together, this evidence indicates that robotic knee perturbations on post-stroke individuals with SKG could elicit counterproductive quadriceps hyperreflexia initiated by suprathreshold RF fiber stretch. Hyperreflexia modeling has been based on muscle fiber length and velocity [26, 47] since spindle proprioceptors encode information for muscle length and velocity changes [23, 28]. Thus, exoskeletal knee flexion assistance that induced hyperreflexia was influenced by increased RF fiber stretch velocity. If RF fiber stretch velocity could be detected and then avoided, it may be possible to enable the full benefits of exoskeletal assistance in those with post-stroke SKG. Real-time measurement of fiber stretch velocity requires difficult to access equipment such as ultrasound and a real-time analysis and control system [31], including other significant challenges of human-in-the-loop control [39]. However, similar to aforementioned work that controlled kinetic and kinematic correlates of metabolic cost [40], it may be possible to indirectly reduce hyperreflexia via optimization of clinically accessible correlates of fiber stretch velocity.

The objective of this study was to determine to what degree kinematic and kinetic features could substitute for RF fiber stretch velocity in predicting hyperreflexive RF muscle activation following exoskeletal assistance. To achieve this, we performed parametric and nonparametric multivariate regression analyses for variable selection on a knee exoskeleton gait data from 8 post-stroke participants with SKG [43]. We hypothesized that hip and knee flexion kinematics would predict RF hyperreflexia due to the biarticular characteristics of the RF. This work represents a novel statistical and machine learning regression approach to identify predictors of hyperreflexia. Obtaining clinically accessible predictors for hyperreflexia will lead to more effective human-in-the-loop assistive strategies that account for neural impairments.

Materials and Methods

Experimental Data

We obtained previously collected data from 8 chronic, hemiparetic participants with post-stroke SKG who gave written informed consent using procedures approved by the local Institutional Review Board [42]. Inclusion criteria for the hemiparetic participants included their peak paretic knee flexion during swing was at least 15° less than their peak nonparetic knee flexion and the ability to walk for 20 min without rest at 0.55 m/s on a treadmill. A lightweight, powered knee orthosis was used to provide knee flexion torque perturbations during the pre-swing phase without affecting the remainder of the gait cycle [43]. Analog data, including ground reaction force (GRF) from the instrumented split-belt treadmill and applied torque by the powered orthosis, were acquired at 1 kHz. Motion capture data on the lower limbs was collected at 120 Hz. Electromyography (EMG) from the RF muscle was measured at 1 kHz.

The experimental protocol involved steps with and without pre-swing knee flexion assistance. Steps with knee flexion assistance ranged from 10 to 40 Nm in peak torque. A mean of less than 1 Nm of resistance was measured on the knee for the remainder of the gait cycle. The weight of the device did not alter walking kinematics [42]. In this study, a total of 406 gait cycles were extracted including 260 gait cycles with knee flexion assistance (Mean ± SD: 23.32 ± 5.85 Nm; Min: 11.40 Nm; Max 34.51 Nm). Previous work describes further details of the protocol [42].

Musculoskeletal Modeling and Simulation

In order to determine muscle–tendon states (i.e., RF muscle fiber stretch velocity at each time instance), we employed musculoskeletal modeling and simulation through OpenSim 4.3 [13] using a method validated in previous work [2, 4]. To summarize, we condensed upper body segments in the gait 2392 model of OpenSim to the pelvis segment to account for a lower body marker set, so that it had 18 degrees of freedom and 90 muscle–tendon actuators. The modified model was scaled to match the anthropometry of each subject. Marker data were fed into the inverse kinematics tool, which generated joint kinematics with the least square fit of marker trajectories. A residual reduction algorithm (RRA) adjusted the model to minimize dynamic inconsistencies between the experimental GRFs and body segment kinematics. Based on the adjusted model after RRA, computed muscle control (CMC) [44] estimated muscle–tendon states and excitation patterns that reproduced the motion while minimizing the sum of excitations squared. The simulated muscle activations are descriptive and derived from distributed joint forces and kinematics with acceptable range of residuals and matching with active EMG regions [2]. Unmeasured handrail forces were estimated as previously described [3]. The dynamic consistency of the simulations was evaluated by examining the resulting residual forces and moments and verifying them with the OpenSim guidelines [21].

Dependent Variable

The dependent variable for the regression analysis was RF activity. The raw RF EMG signals were filtered with a fourth-order band-pass Butterworth filter with cutoff frequencies of 20–400 Hz to remove artifacts, demeaned, rectified, and low-pass filtered with a 4th order Butterworth filter at 10 Hz. To reduce inter-individual variability, we used the mean of the EMG envelope in the trial as the normalization reference for both assisted and unassisted trials [11]. The processed signals were divided into gait cycles based on a paretic limb heel-strike event using vertical GRFs and then normalized into 100-time frames. A reflex response would occur within 120 ms after stimulus onset through mono- or polysynaptic mechanisms [34]. This time interval has been employed to detect quadriceps stretch reflexes following mechanical knee perturbations during gait [29]. In addition to the 120 ms window, we accounted for timing errors from computation of RF fiber stretch velocity and evaluated windows of 90 ms and 150 ms. We defined the initiation of reflex as the timing of the peak pre-swing muscle fiber stretch velocity. Fiber velocity, estimated from the musculoskeletal simulation, served as a proxy for velocity sensitive muscle spindles which initiate the stretch reflex. Our earlier work showed that peak fiber stretch velocity was a reasonably accurate indicator of stretch reflex timing [2]. We then numerically integrated the RF EMG envelopes following stimulus onset to obtain integrated EMG (iEMG) measures representing an involuntary response. Figure 1 visualizes experimental setup and RF iEMG for involuntary responses resulting from exoskeletal assistance.

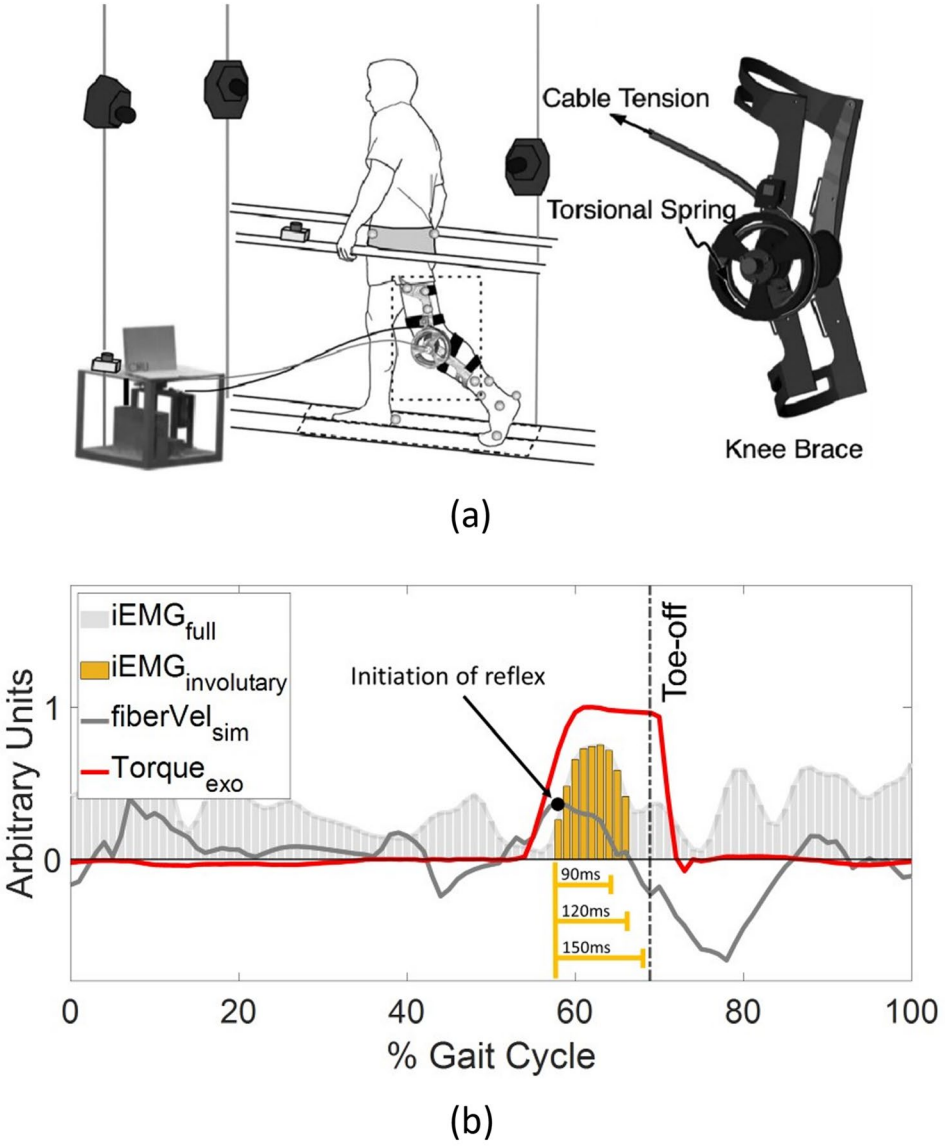

Fig. 1 Visualization of **a** experimental setup with powered knee orthosis [42] and **b** the rectus femoris EMG signals, knee flexion torque assistance, and simulated RF muscle fiber stretch velocity. In **b**, Gray line indicates simulated RF fiber velocity. Red solid line represents the external knee torque assistance profile by the powered knee exoskeleton device. Vertical bars show iEMG of RF. The involuntary response is captured from the peak simulated RF fiber velocity until 120 ± 30 ms following (yellow)

Independent Variables

A total of 14 predictors were extracted from each gait cycle based on muscle–tendon states as well as gait kinematic and kinetic data. One muscle–tendon relevant variable was selected from the musculoskeletal simulation: the peak pre-swing RF fiber stretch velocity. Three variables from hip and knee joint kinematics in the pre-swing phase (i.e., peak hip flexion and knee flexion velocity, and relative peak knee flexion velocity to peak hip flexion) were chosen due to the biarticular physiology of the RF and its associations with post-stroke SKG [18]. Correspondingly, we used body kinematics which are velocities and accelerations based on the configuration (center of mass position and orientation) of each body segment. Specifically, we used 3 body kinematic variables from the thigh and shank segments (i.e., peak thigh and shank angular velocity, and relative peak shank angular velocity to peak thigh) in the pre-swing phase because they could be alternative measures of knee joint kinematics. Besides kinematic features, we selected propulsive/brake impulse because its associations with post-stroke gait deficits including SKG [5, 10]. Specifically, we computed the paretic limb's propulsive, braking, and net impulse during the pre-swing phase [8]. We additionally choose GRF since it is a fundamental components of propulsive/brake impulse [8]. GRF signals were processed to obtain the peak anterior/posterior GRF in the pre-swing phase, peak medial/lateral GRF in the stance phase, and peak vertical GRF in the stance phase. Additionally, we used the pelvic segment acceleration in the anteroposterior plane as a proxy for body acceleration which is highly correlated to net propulsion impulse [5, 9]. The list of parameters is summarized in Table 1 and is visualized in Online Fig. A1.

Variable Selection

Variable selection is a procedure to select appropriate variables from a complete list of variables by removing those that are irrelevant or redundant. This step could be achieved by either parametric or nonparametric regression. The parametric approaches provide generalizable and interpretable statistical inference but require assumptions of linearity and normal distribution. Conversely, nonparametric machine learning methods do not need stringent distribution assumptions, but their models are less interpretable and risk overfitting without optimal tuning of hyper-parameters. In this study, we aimed to achieve a comprehensive variable selection by utilizing both parametric and nonparametric regression methods to address unknown variable relationships.

As a parametric approach, we deployed the least absolute shrinkage and selection operator (LASSO) method which is a popular penalized regression technique that uses an L1-norm penalty on the regression coefficients [45]. By the addition of the regularization term on linear regression, the LASSO regression produces a sparse and interpretable linear model with important variables automatically selected. Here we implemented LASSO with a linear mixed model with the *glmmLasso* package in R statistical software [19]. We set a random intercept model with subjects as random effects and all predictors as fixed effects. We then built repeated fivefold cross-validation to avoid a bias in the evaluation regression model. In data splitting, stratified sampling was applied based on subjects to obtain a sample population that best represents the entire population. In every cross-validation loop, the parameter λ was tuned by grid search using Bayesian Information Criteria (BIC). To quantify the importance of each predictor variable in regression, we ranked variables

Table 1 List of parameters

Description	Abbreviation	Category
Peak rectus femoris fiber stretch velocity in pre-swing [2] (m/s)	RectusFemoris_Vel	Muscle–tendon mechanics
Peak hip flexion velocity in pre-swing (rad/s)	HipFlex_Vel	Joint kinematics
Peak knee flexion velocity in pre-swing [33] (rad/s)	KneeFlex_Vel	Joint kinematics
Relative peak knee flexion velocity with respect to peak hip flexion (rad/s)	relKneeHip_Vel	Joint kinematics
Peak pelvic segment anterior/posterior acceleration in pre-swing [9] (m/s^2)	Pelvic_AntPost_Acc	Body kinematics
Peak thigh segment angular velocity in pre-swing (rad/s)	Thigh_Vel	Body kinematics
Peak shank segment angular velocity in pre-swing (rad/s)	Shank_Vel	Body kinematics
Relative peak shank angular velocity with respect to thigh (rad/s)	relShankThigh_Vel	Body kinematics
Paretic propulsive impulse in pre-swing [8] (%BW · s)	Propulsive_Impulse	Impulse
Paretic braking impulse in pre-swing [8] (%BW · s)	Braking_Impulse	Impulse
Paretic net impulse in pre-swing [8] (% BW · s)	Net_Impulse	Impulse
Peak anterior/posterior ground reaction force in pre-swing (% BW)	AntPost_GRF	GRF
Peak mediolateral GRF in stance (% BW)	MedLat_st_GRF	GRF
Peak vertical GRF in stance (% BW)	Vert_st_GRF	GRF

BW body weight

based on the selection proportions defined by frequencies of each selected variable in trained LASSO models from repeated cross-validation. The selection proportions have a score ranging from 0 (always shrunk, unimportant feature) to 1 (never shrunk, essential feature) by averaging variable selection frequencies so that we could infer individual feature importance in the regression model. The same ranking method was used in a previous regression study for post-stroke clinical outcomes [27]. In this study, we repeated 50 cross-validation repetitions to obtain variable selection proportions from the LASSO regression analysis. Variables above the threshold were determined as critical parameters for prediction. The threshold was 0.95 meaning 95% of the chance for selection across repeated cross-validation.

As an alternative to linearity assumptions, we deployed the non-parametric Bayesian Additive Regression Trees (BART), an ensemble method of regression tree models [12]. BART combines the advantages of the Bayesian model, incorporating past information about a parameter and forming a prior distribution for future analysis, and ensemble methods. It recently has gained popularity due to its superior prediction performance over other machine learning techniques (i.e., random forests, gradient boosting model, neural networks) in various study settings [12, 22]. To evaluate the relative importance of each predictor variable from BART, Chipman et al. proposed the variable inclusion proportion corresponding to the proportion of times each variable is selected for splitting nodes across Markov chain Monte Carlo iterations in the sum-of-trees model [12]. Intuitively, variables with higher inclusion proportions are the more important variables in prediction. In this study, we implemented BART and extracted the variable inclusion proportions as a feature importance metric using the *BART* package publicly available in R statistical software [41]. We performed a repeated fivefold cross-validation with a total of 50 repetitions for unbiased regression outcomes. The stratified split dataset across repetitions was the same as the one used for glmmLASSO for a lateral comparison. Variables above the threshold, denoted by 1/(total number of predictors), were determined as a crucial subset. This threshold stands for the probability of equal inclusion for all predictors in the model.

Reduced Model Selection

With key variables resulting from both parametric and non-parametric variable selection, we fit reduced models using a linear mixed and BART regression. For linear mixed model regression, we formulated a random intercept model with nested random effects in terms of subjects and exoskeletal assistance. Parametric and nonparametric models were compared to each other based on goodness-of-fit measures, such as adjusted R^2 and root mean square error (RMSE) acquired by 50 repetitions of fivefold cross-validations. Based on the reduced fit model, we additionally performed a model selection through backward stepwise elimination. The stepwise elimination on the parametric model was based on the Akaike information criterion (AIC). The adjusted R^2 was used for the nonparametric model's stepwise elimination. This stepwise regression eliminated insignificant variables resulting in the final best fit model with minimum numbers of predictors. Additionally, the relationships between variables were examined by correlation analysis to investigate the importance of individual predictors. Spearman's rank correlation coefficient was used due to its reliability in case the data was not normally distributed. The overall workflow is summarized in Fig. 2.

Results

Parametric and non-parametric models showed similar results (Fig. 3)**.** Four parameters from kinematic and muscle–tendon state variables in the pre-swing phase remained (> 95% of selection proportion) in the LASSO model across all 50 iterations: peak shank velocity, relative peak knee velocity with respect to hip, peak RF fiber stretch velocity, and peak knee flexion velocity. The same four variables were identified using BART, with the addition of the peak RF fiber stretch velocity and the peak knee flexion velocity. All parameters above the significance threshold using LASSO were also above the significance threshold using BART. Both variable selections resulted in low importance scores for all variables related to GRF and impulse.

To ensure the model was both representative and not overly complex, we fitted a reduced model using all six significant predictors from Fig. 3, and then evaluated the goodness-of-fit of models. We used the same random effects and the same hyperparameter setting as the variable selection. Table 2 summarizes accuracy measures for full and reduced regression models from repeated fivefold cross-validation. The reduced model showed slightly degraded goodness-of-fit (i.e., increased RMSE and decreased adjusted R^2) compared to the full model. Except for the parametric regression model's out-of-bag test, all accuracy measurements differed significantly between full and reduced models ($p < 0.001$).

Backward stepwise elimination additionally cut down the number of variables from the reduced model of six important predictors. Stepwise regression using the parametric linear mixed model determined the last four crucial variables including two joint kinematic and another two body kinematic variables: peak hip flexion velocity, relative peak knee velocity to peak hip flexion, peak shank velocity and the relative peak shank velocity to peak thigh velocity. Table 3 represents the summary of the final regression model by a random intercept mixed model with nested random effects

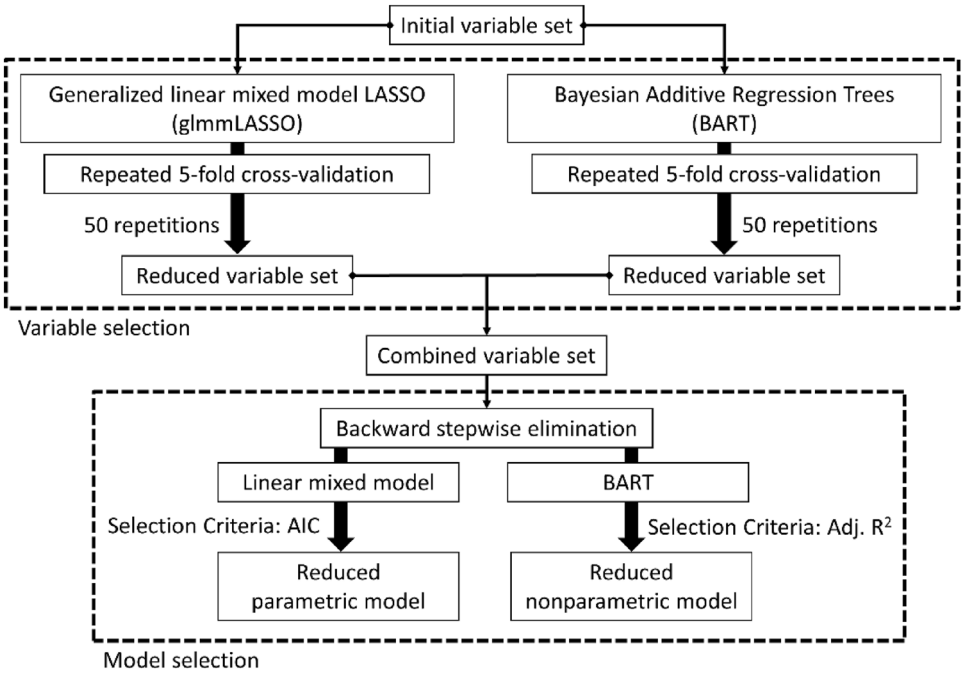

Fig. 2 Overall workflow. *AIC* akaike information criterion; *Adj.* R^2 adjusted R^2

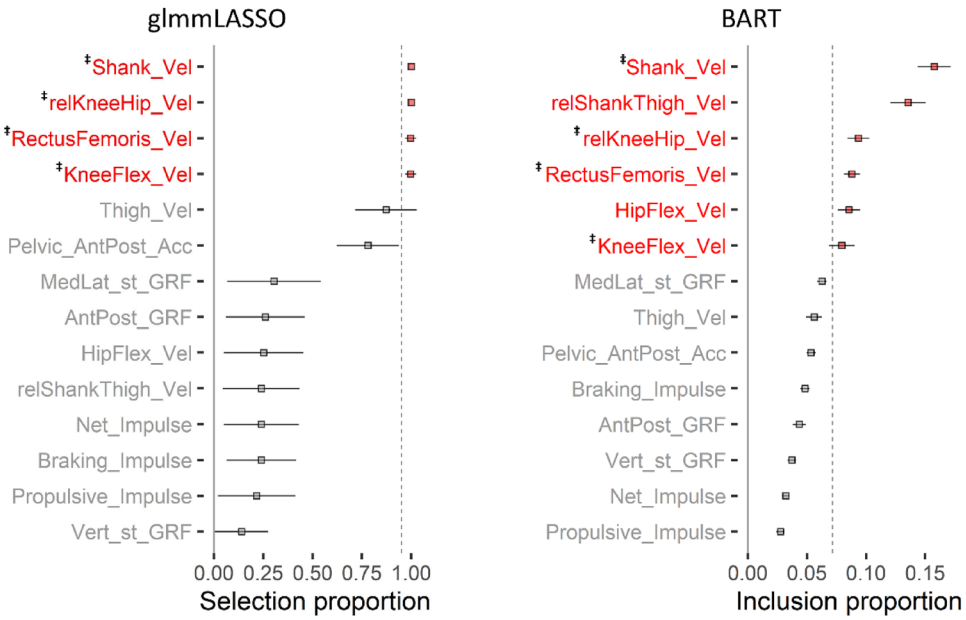

Fig. 3 Variable selection results from glmmLASSO (left) and BART (right) for a total of 14 predictors. The square markers represent the average, and the solid lines are the standard deviation of total 50 repetitions. The red-colored variables are essential variables showing above threshold (vertical dashed line) denoted by 95% of selection proportions and 1/total number of variables for glmmLASSO and BART, respectively. The common essential variables between methods denoted by superscript symbol of ‡

Table 2 Summary of regression model accuracy (Mean ± SD) from repeated fivefold cross-validation

No. predictors	glmmLASSO		BART	
	14 ($Model_{Full}$)	6 ($Model_{Reduced}$)	14 ($Model_{Full}$)	6 ($Model_{Reduced}$)
RMSE (A.U.)				
Train	5.20 ± 0.01	**5.39 ± 0.07**	3.12 ± 0.08	**3.86 ± 0.04**
Test	5.68 ± 0.06	5.64 ± 0.06	5.41 ± 0.11	**5.52 ± 0.08**
Adj. R^2				
Train	0.47 ± 0.00	**0.43 ± 0.00**	0.83 ± 0.01	**0.73 ± 0.01**
Test	0.40 ± 0.11	0.41 ± 0.01	0.46 ± 0.02	**0.43 ± 0.02**

Highlighted as bold indicates the model accuracy significantly changed from the full model

Table 3 Summary of final model from stepwise backward regression

Marginal R^2/Conditional R^2: 0.074/0.505 Adjusted R^2: 0.533		Slope estimates	[95% CI]
Category	Predictors		
Joint kinematics	HipFlex_Vel [rad/s]	11.30**	[2.61, 19.98]
	relKneeHip_Vel [rad/s]	11.59*	[3.38, 19.71]
Body kinematics	Shank_Vel [rad/s]	−21.11**	[−37.10, −5.12]
	relShankThigh_Vel [rad/s]	10.54**	[1.96, 19.11]

*$p < 0.05$, **$p < 0.01$ ***$p < 0.001$

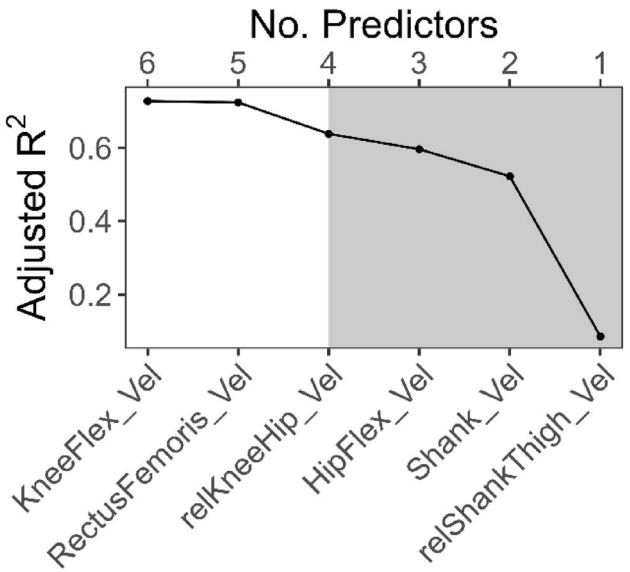

Fig. 4 Goodness-of-fit changes by BART stepwise backward elimination. The variable names shown in the bottom axis are the predictors removed at each step. For example, "KneeFlex_Vel" was removed at the first step of elimination from a model with six variables. The gray shaded area indicates the steps that the adjusted R^2 was significantly affected by the elimination

with respect to subject and assistance. Small marginal R^2 (0.074) but moderate conditional R^2 (0.505) accounted for the most variance of this model. The adjusted R^2 of this final model was 0.533. Backward elimination based on the nonparametric model, BART, revealed the same last four critical predictors. Figure 4 illustrates the goodness-of-fit changes through backward elimination using BART. Once the model consisted of less than four predictors, its adjusted R^2 started decreasing significantly meaning that variables in the gray shaded area of Fig. 4 were the minimum crucial predictor set. The adjusted R^2 of BART model with four variables was 0.638. The results were robust to differences in timing (Online Figs. A2–A4, Tables A1, A2).

The relationships between selected kinematic predictors and muscle–tendon state, pre-swing rectus femoris fiber stretch velocity, were examined by Spearman's rank correlation coefficient. Table 4 summarizes the coefficients. The

Table 4 Spearman's rank correlation coefficient (ρ) between key kinematic predictors and pre-swing rectus femoris fiber stretch velocity

Category	Predictors	ρ
Joint kinematics	HipFlex_Vel [rad/s]	0.59***
	relKneeHip_Vel [rad/s]	0.90***
Body kinematics	Shank_Vel [rad/s]	0.87***
	relShankThigh_Vel [rad/s]	−0.18***

*$p < 0.05$, **$p < 0.01$, ***$p < 0.001$

correlations of involuntary RF activity with the other key kinematic predictors for each individual with and without exoskeletal assistance are shown in Online Fig. A6.

Discussion

Exoskeletal assistance has the potential to unload some of the effort from clinicians and caregivers but does not yet account for other neuromuscular impairments such as hyperreflexia [1, 42]. The aim of this study was to determine accessible biomechanical predictors of quadriceps hyperreflexia based on walking data from those with post-stroke SKG with and without knee flexion exoskeletal assistance. We used both parametric and non-parametric regression techniques to obtain two different perspectives of the key kinematic, kinetic and muscle–tendon predictors of rectus femoris hyperreflexia. We found four kinematic predictors obtained during pre-swing phase were shared between the regression techniques: peak hip flexion velocity, the relative peak knee to peak hip flexion velocity, peak shank angular velocity, and the relative peak shank to peak thigh angular velocity. These parameters can be measured by two or three wearable sensors, and with assumptions, possibly even one [7]. The implication of these findings is that these parameters can be used to predict hyperreflexia, with future potential for control during exoskeletal assistance.

Our group's previous musculoskeletal simulation analysis confirmed the strong association between simulated RF muscle fiber stretch velocity and RF excitability [2]. In this study, both parametric and nonparametric regression techniques for

variable selection resulted in the same finding that kinematic variables are predictive of an RF reflex. Indeed, there were strong correlations ($\rho \simeq 0.90$) between some of the selected predictors (relative peak knee flexion velocity to peak hip flexion velocity, peak shank angular velocity) and RF fiber stretch velocity (Table 4), as we expected. We did not expect that these parameters would be more predictive of a reflex than RF fiber stretch velocity, the physiological mechanism of a stretch reflex. The fiber stretch velocity was computed using generic Hill-type muscle models and mathematically driven cost functions [44], rather than direct measurement, a model validated in our previous work [2]. Yet, it remains possible that RF fiber stretch velocity could have played a stronger statistical role if the true value could have been obtained. Regardless of the level of significance between variables, it is notable that out of all 14 parameters, the ones found to be most predictive of a reflex were ones related to hip and knee kinematics as well as RF fiber stretch velocity. This finding is consistent with our hypothesis that more easily measurable kinematic variables can serve as a proxy for fiber stretch velocity, potentially for use in exoskeletal control.

Over the past decade, the exoskeleton community has moved towards human-in-the-loop design [48], including the incorporation of real-time estimation of musculotendon mechanics [35], and ultrasound imaging [16, 31, 38]. While these approaches provide an exciting potential for the future of personalized robotics, there are significant challenges, including duration of use, donning/doffing and implementation in a clinical population [39]. Human-in-the-loop optimization requires long experiment times to acquire enough data. It is an empirical question of whether pre-recorded gait data in those with post-stroke SKG can provide a sufficient initial guess on a proper reflex threshold. In this work, we found that joint kinematics accurately predict reflex responses in the RF. We estimate that kinematic predictors from this study could be measured by two or even one portable motion sensor such as inertial measurement units. This is significant because it questions the basis for using complex imaging or computational technology in lieu of simpler proxies. Enabling the use of ubiquitous sensor systems would allow exoskeleton engineers and rehabilitation researchers to design practical and effective devices.

This study has several limitations. We made a selection of 14 initial parameters related to post-stroke SKG. Due to the exponential increase in the sampling volume, adding extra dimensionality is not always beneficial in regression analysis, specifically when there are sparse relevant predictors compared to the total number of predictors or the fundamental relationships are nonlinear (so called "curse of dimensionality") [17]. To avoid these adverse effects, we limited the scope of parameter sources among previously assessed associations with post-stroke SKG. Additionally, we did not include parameters that were unable to be directly measured, such as joint kinetics, except for simulated muscle fiber stretch velocity. Therefore, in this work, we aimed to balance comprehensiveness, practicality, and overfitting. Regression approaches based on observations from only 8 participants may affect generalization of the results. Despite the small sample size, the repeated fivefold cross-validation [37] took into account the randomness in sampling resulting in unbiased and trustworthy variable and model selection results. This study does not provide causal relationships between kinematic parameters and quadriceps hyperreflexia. However, it is notable that the predictors of RF hyperreflexia (i.e., related to knee-hip velocities) found in this work were all physiologically related to the biarticular span of the RF suggesting that this statistical approach may help reveal mechanisms of hyperreflexia. For instance, the relative peak angular velocity between the knee and hip was the most correlated variable with RF fiber stretch velocity ($\rho = 0.90$ in Table 4). Still, the relative peak angular velocity between the shank and thigh had a weak negative correlation ($\rho = -0.18$ in Table 4) to RF fiber stretch velocity. While thigh-shank segment and knee-hip joint velocities are not equivalent, the large difference in correlations is difficult to explain mechanistically and interventional approaches could help elucidate these differences. Lastly, our findings were based on two types of regression techniques among numerous statistical and machine learning approaches. Although there exists an advanced penalized regression approach improving the limitations of LASSO [36] (i.e., Elastic Net [49]), glmmLASSO in this study could result in a better model due to subjects' random-effects modeling. There were also popular tree-based machine learning algorithms, such as gradient boosting [30] and random forest methods [6]. It has been reported that BART has outperformed these other methods [12]. Therefore, the use of these two different regression methods was sufficient.

Conclusions

Despite the rapid growth of wearable robot technology, there is still a lack of consideration regarding neuromuscular impairments such as hyperreflexia into device design. In this study, we introduced regression-based variable selection for predicting rectus femoris hyperreflexia following pre-swing knee flexion exoskeletal assistance. We found that four kinematic variables relevant to knee and hip joint motions were sufficient to effectively predict hyperreflexia in people with post-stroke SKG. These results suggest that effective monitoring and control of these accessible knee and hip kinematics may be more productive at regulating hyperreflexia than the more complex acquisition of muscle fiber stretch velocity. This work represents a novel statistical

approach to identifying biomechanical associations with reflex function. This information could be used to further understand the mechanisms of hyperreflexia and its associated clinical interventions.

Supplementary Information The online version contains supplementary material available at https://doi.org/10.1007/s10439-023-03217-x.

Funding This work was supported by the National Center for Medical Rehabilitation Research at the National Institute of Child Health and Human Development under the award number R01HD100416.

Declarations

Conflict of interest The authors declare that they have no conflict of interest.

References

1. Akbas, T., K. Kim, K. Doyle, K. Manella, R. Lee, P. Spicer, M. Knikou, and J. Sulzer. Rectus femoris hyperreflexia contributes to Stiff-Knee gait after stroke. *J. NeuroEng. Rehabil.* 17:117, 2020.
2. Akbas, T., R. R. Neptune, and J. Sulzer. Neuromusculoskeletal simulation reveals abnormal rectus femoris-gluteus medius coupling in post-stroke gait. *Front. Neurol.* 10:301, 2019.
3. Akbas, T., and J. Sulzer. Implementing a virtual gait assistance device within a musculoskeletal simulation framework. 2015.
4. Akbas, T., and J. Sulzer. Musculoskeletal simulation framework for impairment-based exoskeletal assistance post-stroke. 2019. https://doi.org/10.1109/ICORR.2019.8779564
5. Awad, L. N., M. D. Lewek, T. M. Kesar, J. R. Franz, and M. G. Bowden. These legs were made for propulsion: advancing the diagnosis and treatment of post-stroke propulsion deficits. *J. NeuroEng. Rehabil.* 17:139, 2020.
6. Biau, G., and E. Scornet. A random forest guided tour. *TEST*. 25:197–227, 2016.
7. Bonnet, V., V. Joukov, D. Kulić, P. Fraisse, N. Ramdani, and G. Venture. Monitoring of hip and knee joint angles using a single inertial measurement unit during lower limb rehabilitation. *IEEE Sens. J.* 16:1557–1564, 2016.
8. Bowden, M. G., C. K. Balasubramanian, R. R. Neptune, and S. A. Kautz. Anterior–posterior ground reaction forces as a measure of paretic leg contribution in hemiparetic walking. *Stroke*. 37:872–876, 2006.
9. Bowden, M. G., A. L. Behrman, M. Woodbury, C. M. Gregory, C. A. Velozo, and S. A. Kautz. Advancing measurement of locomotor rehabilitation outcomes to optimize interventions and differentiate between recovery versus compensation. *J. Neurol. Phys. Therapy JNPT*. 36:38, 2012.
10. Brough, L. G., S. A. Kautz, and R. R. Neptune. Muscle contributions to pre-swing biomechanical tasks influence swing leg mechanics in individuals post-stroke during walking. *J. NeuroEng. Rehabil.* 19:55, 2022.
11. Burden, A. How should we normalize electromyograms obtained from healthy participants? What we have learned from over 25 years of research. *J. Electromyogr. Kinesiol.* 20:1023–1035, 2010.
12. Chipman, H. A., E. I. George, and R. E. McCulloch. BART: Bayesian additive regression trees. *Ann. Appl. Stat.* 4:266–298, 2010.
13. Delp, S. L., F. C. Anderson, A. S. Arnold, P. Loan, A. Habib, C. T. John, E. Guendelman, and D. G. Thelen. OpenSim: Open-source software to create and analyze dynamic simulations of movement. *IEEE Trans. Biomed. Eng.* 54:1940–1950, 2007.
14. Duncan, P. W., R. Zorowitz, B. Bates, J. Y. Choi, J. J. Glasberg, G. D. Graham, R. C. Katz, K. Lamberty, and D. Reker. Management of adult stroke rehabilitation care. *Stroke*. 36:e100–e143, 2005.
15. Esquenazi, A., M. Talaty, and A. Jayaraman. Powered exoskeletons for walking assistance in persons with central nervous system injuries: A narrative review. *PM&R*. 9:46–62, 2017.
16. Franz, J. R. A sound approach to improving exoskeletons and exosuits. *Sci. Robot.* 2021. https://doi.org/10.1126/scirobotics.abm6369.
17. Geenens, G. Curse of dimensionality and related issues in nonparametric functional regression. *Stat. Surv.* 5:30–43, 2011.
18. Goldberg, S. R., S. Õunpuu, A. S. Arnold, J. R. Gage, and S. L. Delp. Kinematic and kinetic factors that correlate with improved knee flexion following treatment for stiff-knee gait. *J. Biomech.* 39:689–698, 2006.
19. Groll, A., and G. Tutz. Variable selection for generalized linear mixed models by L 1-penalized estimation. *Stat. Comput.* 24:137–154, 2014.
20. Hendricks, H. T., J. van Limbeek, A. C. Geurts, and M. J. Zwarts. Motor recovery after stroke: A systematic review of the literature. *Arch. Phys. Med. Rehabil.* 83:1629–1637, 2002.
21. Hicks, J. L., T. K. Uchida, A. Seth, A. Rajagopal, and S. L. Delp. Is my model good enough? Best practices for verification and validation of musculoskeletal models and simulations of movement. *J. Biomech. Eng.* 2015. https://doi.org/10.1115/1.4029304.
22. Hill, J. L. Bayesian nonparametric modeling for causal inference. *J. Comput. Graph. Stat.* 20:217–240, 2011.
23. Houk, J. C., W. Z. Rymer, and P. E. Crago. Dependence of dynamic response of spindle receptors on muscle length and velocity. *J. Neurophysiol.* 46:143–166, 1981.
24. Jørgensen, H. S., H. Nakayama, H. O. Raaschou, and T. S. Olsen. Recovery of walking function in stroke patients: The Copenhagen stroke study. *Arch. Phys. Med. Rehabil.* 76:27–32, 1995.
25. Kalita, B., J. Narayan, and S. K. Dwivedy. Development of active lower limb robotic-based orthosis and exoskeleton devices: A systematic review. *Int. J. Soc. Robot.* 13:775–793, 2021.
26. Le Cavorzin, P., S. A. Poudens, F. Chagneau, G. Carrault, H. Allain, and P. Rochcongar. A comprehensive model of spastic hypertonia derived from the pendulum test of the leg. *Muscle Nerve*. 24:1612–1621, 2001.
27. Majeed, Y. A., S. S. Awadalla, and J. L. Patton. Regression techniques employing feature selection to predict clinical outcomes in stroke. *PLoS ONE*.13:e0205639, 2018.
28. Matthews, P. B. C. The response of de-efferented muscle spindle receptors to stretching at different velocities. *J. Physiol.* 168:660–678, 1963.
29. Mrachacz-Kersting, N., B. A. Lavoie, J. B. Andersen, and T. Sinkjaer. Characterisation of the quadriceps stretch reflex during the transition from swing to stance phase of human walking. *Exp. Brain Res.* 159:108–122, 2004.
30. Natekin, A., and A. Knoll. Gradient boosting machines, a tutorial. *Front. Neurorobotics*. 2013. https://doi.org/10.3389/fnbot.2013.00021.
31. Nuckols, R. W., S. Lee, K. Swaminathan, D. Orzel, R. D. Howe, and C. J. Walsh. Individualization of exosuit assistance based on measured muscle dynamics during versatile walking. *Sci. Robot.* 2021. https://doi.org/10.1126/scirobotics.abj1362.
32. Perry, J., and J. M. Burnfield. Gait Analysis: Normal and Pathological Function. Thorofare: Slack, 1992.
33. Piazza, S. J., and S. L. Delp. The influence of muscles on knee flexion during the swing phase of gait. *J. Biomech.* 29:723–733, 1996.
34. Pierrot-Deseilligny, E., and D. Burke. The Circuitry of the Human Spinal Cord: Its Role in Motor Control and Movement Disorders. Cambridge: Cambridge University Press, 2005.

35. Pizzolato, C., D. G. Lloyd, M. Sartori, E. Ceseracciu, T. F. Besier, B. J. Fregly, and M. Reggiani. CEINMS: A toolbox to investigate the influence of different neural control solutions on the prediction of muscle excitation and joint moments during dynamic motor tasks. *J. Biomech.* 48:3929–3936, 2015.
36. Ranstam, J., and J. A. Cook. LASSO regression. *Br. J. Surg.* 105:1348, 2018.
37. de Rooij, M., and W. Weeda. Cross-validation: A method every psychologist should know. *Adv. Methods Pract. Psychol. Sci.* 3:248–263, 2020.
38. Sheng, Z., A. Iyer, Z. Sun, K. Kim, and N. Sharma. A hybrid knee exoskeleton using real-time ultrasound-based muscle fatigue assessment. *IEEE/ASME Trans. Mechatron.* 2022. https://doi.org/10.1109/TMECH.2022.3171086.
39. Siviy, C., L. M. Baker, B. T. Quinlivan, F. Porciuncula, K. Swaminathan, L. N. Awad, and C. J. Walsh. Opportunities and challenges in the development of exoskeletons for locomotor assistance. *Nat. Biomed. Eng*. 2022. https://doi.org/10.1038/s41551-022-00984-1.
40. Slade, P., M. J. Kochenderfer, S. L. Delp, and S. H. Collins. Personalizing exoskeleton assistance while walking in the real world. *Nature*. 610:277–282, 2022.
41. Sparapani, R., C. Spanbauer, and R. McCulloch. Nonparametric machine learning and efficient computation with Bayesian additive regression trees: The BART R package. *J. Stat. Softw.* 97:1–66, 2021.
42. Sulzer, J. S., K. E. Gordon, Y. Y. Dhaher, M. A. Peshkin, and J. L. Patton. Preswing knee flexion assistance is coupled with hip abduction in people with stiff-knee gait after stroke. *Stroke*. 41:1709–1714, 2010.
43. Sulzer, J. S., R. A. Roiz, M. A. Peshkin, and J. L. Patton. A highly backdrivable, lightweight knee actuator for investigating gait in stroke. *IEEE Trans. Robot.* 25:539–548, 2009.
44. Thelen, D. G., and F. C. Anderson. Using computed muscle control to generate forward dynamic simulations of human walking from experimental data. *J. Biomech.* 39:1107–1115, 2006.
45. Tibshirani, R. Regression shrinkage and selection via the lasso. *J. R. Stat. Soc. Series B (Methodological)*. 58:267–288, 1996.
46. Young, A. J., and D. P. Ferris. State of the art and future directions for lower limb robotic exoskeletons. *IEEE Trans. Neural Syst. Rehabil. Eng.* 25:171–182, 2017.
47. Young, R. R. Spasticity: A review. *Neurology*. 44:S12-20, 1994.
48. Zhang, J., P. Fiers, K. A. Witte, R. W. Jackson, K. L. Poggensee, C. G. Atkeson, and S. H. Collins. Human-in-the-loop optimization of exoskeleton assistance during walking. *Science*. 2017. https://doi.org/10.1126/science.aal5054.
49. Zou, H., and T. Hastie. Regularization and variable selection via the elastic net. *J. R. Stat. Soc. Series B (Statistical Methodology)*. 67:301–320, 2005.